# Development of an Active Load Cell Force Measurement Test Rig

Paul Gancitano [a], Benstone Schwartz [a], Roger Fittro[a], Carl Knospe [a]

[a] University of Virginia, Department of Mechanical & Aerospace Engineering, Charlottesville, VA, USA, rlf9w@virginia.edu

***Abstract*—As industrial machine performance requirements progress, accurate high frequency fluid-film bearing coefficients are necessary in order to ensure accurate prediction of system level machine rotordynamics. Traditional fluid-film bearing test rigs have been shown to enable accurate dynamic bearing coefficient identification. However, the uncertainty of these coefficients significantly increase at higher frequencies (>250 Hz). Therefore, as modern high performance machinery require high accuracy high frequency dynamic coefficient validation, a new bearing test rig design is required. This work solves this problem through the development of a new test rig based on the development of an "Active Load Cell". The theoretical development, test rig design and detailed simulation results are presented to demonstrate the dynamic force measurement performance capabilities of an Active Load Cell over a broad frequency range.**

## INTRODUCTION

In many industrial machines - such as gas turbines, steam turbines and compressors - fluid-film bearings are used to support the rotating shafts. System-level performance requirements are trending toward higher rotating speeds and higher load conditions. Accurate knowledge of fluid-film bearing stiffness and damping coefficients are critical to the accurate prediction of the dynamic behavior of these machines. Fluid-film bearing coefficients are modeled with bearing codes such as state-of-the-art thermoelastohydrodynamic (TEHD) codes [1] and included in rotordynamic analyses.

Modeling bearings accurately is a challenging task and Kocur et al. found in an API-sponsored survey that predictions of stiffness and damping coefficients varied by almost an order of magnitude [2]. The survey requested the coefficients for a bearing design which was sent to engineers and researchers working with fluid-film bearings. Steps were taken to isolate differences in bearing models as the cause of variation by providing a common rotor model and damped eigenvalue solution algorithm. This resulted in variations of predicted damped eigenvalues being attributed to variations in predicted coefficients. Ultimately, one of the conclusions from the Kocur et al. survey is that "a gold standard of experimental data is needed" to validate component coefficient predictions. With more reliable data, bearing models can be validated and variation in predictions can be reduced.

Previous test rigs have been developed for the purpose of experimentally identifying these bearing dynamic coefficients [3]. The literature review suggests that uncertainty in the experimentally identified coefficients is not typically addressed. When a measure of uncertainty is presented, it's often an analysis of repeatability or a measure of curve fit quality. Repeatability analysis is insufficient to understand the uncertainty in identified coefficients because it is an analysis of random errors and in principle, random errors can be minimized by taking more samples. Systematic errors, however lead to unavoidable error in identified coefficients. The addition of quality of curve fit is not sufficient to analyze the effects of systematic error on the experiment. Simply stated, comprehensive analysis of the effect of systematic errors on coefficient identification is uncommon.

To address this, Schwartz et al. [4] extended a method developed by Kostrzewsky et al. [5] to model experimental coefficient uncertainty due to systematic errors over a range of test frequencies for a system operating at a constant speed. The analysis was based on the typical identification experiment where force measurements applied to the system and relative displacement measurements between rotor and stator are used to identify coefficients. Using a single-axis representation as an initial simplified model, analytical equations for coefficient identification errors were developed that established trends in uncertainty and showed that the inertial component causes uncertainty to increase quadratically as a function of excitation frequency. This behavior can increase uncertainty rapidly beyond useful bounds for higher-frequency excitations. In addition, the analysis showed that attempting to compensate for the inertia of the excited component in the experiment could actually increase uncertainty due to the additional acceleration measurement error.

Current methods of force identification are indirect and subject to measurement errors that compound at higher frequencies to create significant uncertainties in the identified values. The "Active Load Cell" is a new experimental method of determining fluid-film bearing forces without the need for inertial correction [11]. An adaptive control algorithm [6, 7, 8] works in conjunction with accelerometer readings and an electrodynamic shaker to adaptively cancel the motion of the bearing housing. This measurement method has the potential to determine bearing forces directly, and to a higher degree of accuracy than previous force identification methods. This research details the development and simulation of an Active Load Cell (ALC) Test Rig, which will be used to validate this concept. The simulation results

documented in this paper suggest that bearing force amplitude and phase can be determined within 1% of true values across a wide range of test frequencies, bearing stiffness, and dynamic loading conditions. Determining bearing force within 1% of the true value can in turn lead to significant improvements in bearing dynamic coefficient identification uncertainty.

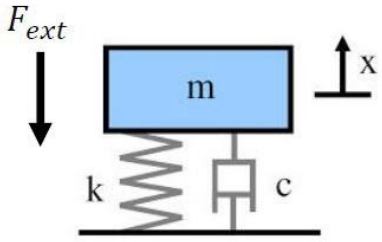


Figure 1. Single mass system with external applied force

## THEORETICAL DEVELOPMENT

Test rigs for determining bearing coefficients typically utilize a measurement of the force applied to the excited component and the relative displacement between the excited and rigidly held component. Schwartz et al. developed a single axis, single degree-of-freedom model (Figure 1) of this experimental technique [4]. Starting with the mathematical representation of the identification in the frequency domain:

$$\frac{F}{X} = (k - m\omega^2) + jc\omega \tag{1}$$

Measurement errors can be applied with the following model:

$$\bar{X} = (1 + \Delta_x)X$$
$$\bar{F} = (1 + \Delta_f)F \tag{2}$$

$\Delta_x$ and $\Delta_f$ are complex numbers representing errors in measured amplitude and phase of the true signal. When the measured signals are utilized in the identification process, the identified coefficients ($\bar{k}$ and $\bar{c}$) are different from truth (k and c):

$$\frac{\bar{F}}{\bar{X}} = (\bar{k} - m\omega^2) + j\bar{c}\omega \tag{3}$$

Through substitution, the identified coefficients can be equated to the true coefficients and then through algebraic manipulations, the uncertainty representations can be written as follows:

$$\frac{\bar{k} - k}{k} = Re(\Delta_{tot})\left(1 - \frac{m\omega^2}{k}\right) - Im(\Delta_{tot})\left(\frac{c\omega}{k}\right)$$
$$\frac{\bar{c} - c}{c} = Re(\Delta_{tot}) + Im(\Delta_{tot})\left(\frac{k}{c\omega} - \frac{m\omega}{c}\right) \tag{4}$$

The exact simplification from $\Delta_x$ and $\Delta_f$ to $\Delta_{tot}$ can be seen in reference [4]. It can be seen that the inertia of the excited component plays a role in the error of the identified coefficient. This leads to high uncertainties at high frequencies, especially above the rotor-bearing system's natural frequency where inertia dominates the dynamics.

However, if instead of identifying the dynamic coefficients via the applied force on the system, the bearing force is directly measured, the inertial term no longer plays a role in the uncertainty. The Active Load Cell concept proposes to enable this by accurately identifying the bearing force directly. The fundamental model for the ALC introduces a second degree of freedom – an additional component which does not have the dynamic excitation force directly applied to it. Consider the two-mass system with two external forces depicted in Figure 2.

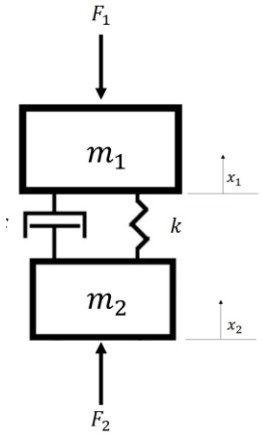


Figure 2: Two mass system with two external forces

The equations of motion for the two masses in this system can be written as equations 5 and 6.

$$m_1\ddot{x}_1 = -F_1 + k(x_2 - x_1) + c(\dot{x}_2 - \dot{x}_1) \tag{5}$$

$$m_2\ddot{x}_2 = F_2 - k(x_2 - x_1) - c(\dot{x}_2 - \dot{x}_1) \tag{6}$$

where $F_1$ and $F_2$ are externally applied forces. $F_1$ represents a dynamic excitation force applied to the system. $F_2$ represents the force applied via the Active Load Cell. Another force, $F_b$, can also be defined such that

$$F_b = k(x_2 - x_1) + c(\dot{x}_2 - \dot{x}_1) \tag{7}$$

which represents the force of a fluid-film bearing connecting the two masses. Substituting (7) into (5) and (6) results in:

$$m_1\ddot{x}_1 = -F_1 + F_b \tag{8}$$

$$m_2\ddot{x}_2 = -F_b + F_2 \tag{9}$$

By observation, when the acceleration of the mass, $m_2$, is exactly zero, the forces acting on the body, $F_b$ and $F_2$ are equivalent. It is also important to note that in this case, the value of $F_b$ can be determined without any knowledge of $F_1$, and with an accuracy based on the precision with which the input force $F_2$ is known. Therefore by controlling the external

force, $F_2$, such that the acceleration of $x_2$ is driven to zero, an accurate measurement of $F_b$ can be made.

Noting that bearing coefficient identification experiments utilize the relative displacement between the rotor and stator:

$$x_2 - x_1 = x_m \qquad (10)$$

$$\dot{x}_2 - \dot{x}_1 = \dot{x}_m \qquad (11)$$

This changes the frequency domain mathematical identification model to the form:

$$\frac{F_b}{X_m} = k + jc\omega \qquad (12)$$

Following the same process of applying measurement error modeling from [4] yields the following expression for dynamic coefficient identification uncertainty:

$$\frac{\bar{k} - k}{k} = Re(\Delta_{tot}) - Im(\Delta_{tot})(\frac{c\omega}{k})$$
$$\frac{\bar{c} - c}{c} = Re(\Delta_{tot}) + Im(\Delta_{tot})(\frac{k}{c\omega}) \qquad (13)$$

These equations demonstrate that by measuring the bearing force via the Active Load Cell, identification uncertainty grows linearly as a function of frequency rather than quadratically, allowing for more accurate validation of bearing models at higher frequencies.

## CONTROL SYSTEM ARCHITECTURE

A simplified schematic of an Active Load Cell based Fluid Film Bearing Test Rig (FFBTR) is shown in Figure 3 and consists of the following components: i) rotor, ii) fluid-film bearing, iii) active magnetic bearings to provide both static and dynamic loading, iv) an array of magnetic actuators supporting the bearing housing, and v) an electrodynamic shaker.

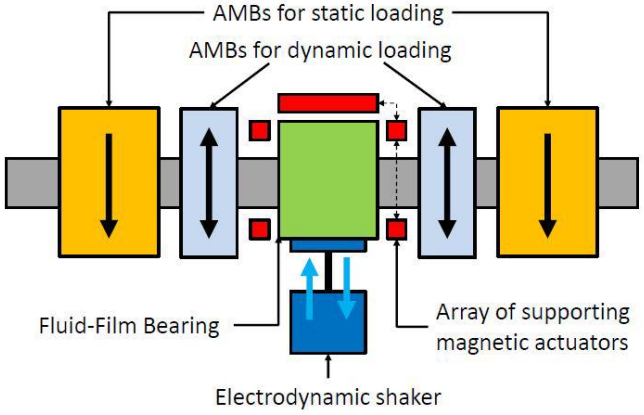


Figure 3: Fluid Film Bearing Test Rig with Active Load Cell

Unlike other bearing test rigs, knowledge of the excitation forces applied to the rotor (or stator) are not used in order to experimentally identify the fluid-film bearing dynamic coefficients (stiffness and damping). Instead, the electrodynamic shaker is used to determine the bearing force directly. This shaker is responsible for providing dynamic, adaptive cancellation forces directly on the bearing housing, which results in zeroing out the motion of the housing and thus exactly cancelling out/identifying the force applied by the bearing ($F_b$).

The configuration in Figure 3 represents a test rig that focuses on single-frequency identification experiments for fluid-film bearings. The array of supporting magnetic actuators behave like magnetic bearings supporting the bearing stator for all frequencies other than the test frequency. A notch filter or adaptive cancellation algorithm [6] can be used to nullify the supporting actuator force contribution at the test frequency such that only the electrodynamic actuator is acting at the frequency of interest. Thus, the only forces measured by the Active Load Cell are those that the bearing is exerting at the selected excitation frequency.

The components which comprise the Active Load Cell in relation to the FFBTR depicted in Figure 3 are: i) electrodynamic shaker; ii) one (or more) accelerometers on the bearing housing; and iii) a current sensor on the shaker. The block diagram in Figure 4 represents the high-level interaction between the Active Load Cell test rig components. This system model is helpful in understanding the construction of the test rig, as well as the simulation model to be discussed in later sections.

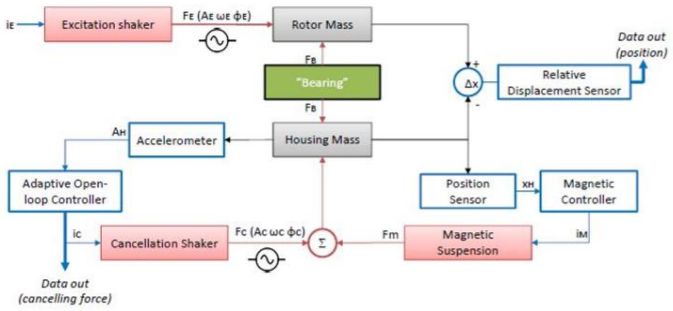


Figure 4: Block diagram representation of Active Load Cell System

Following the flow of the block diagram in Figure 4, the excitation shaker provides a dynamic force at a given test frequency, amplitude, and bias (static load). In the FFBTR, this would represent the static load supported by the fluid-film bearing plus the dynamic excitation experienced by the bearing. This force is directly applied to the rotor mass which represents the inertia of the rotor in the FFBTR. The bearing, which is situated between the rotor and housing masses, provides an equal and opposite force between these bodies arising from the mechanics of the bearing (i.e. hydrodynamic force for a fluid-film bearing). The housing mass also has an electrodynamic shaker coupled to it which produces the cancellation force at the same frequency, but with an amplitude and phase as dictated by an adaptive cancellation algorithm [6]. The overall control system features two independent control loops. The first control loop provides stabilization of the housing position at all frequencies that are not the test frequency. The second control loop takes data

from the accelerometer(s) mounted to the housing body and uses this information to adaptively adjust the amplitude and phase of the electrodynamic shaker. This controller is responsible for altering the current into the cancellation shaker to adaptively match the bearing force applied to the housing at the applied test frequency. The identified bearing force is in the form:

$$F_b(t)=A_b \cos(\omega_b t + \phi_b) \quad (14)$$

## TEST RIG DESIGN

In order to validate the active load cell concept before applying it to a fluid-film bearing test rig, a simplified Active Load Cell test rig was first developed. A conceptual design of this test rig is shown in Figure 5. The major test rig components are as follows: i) Rotor Mass; ii) Housing Mass; iii) Bearing; iv) Excitation Shaker; v) Cancellation Shaker; vi) 3 DOF Magnetic Bearing; vii) Flexures. The test rig is roughly 1.2 m (48 in) tall. And in order to design the ALC test rig to roughly replicate the associated fluid-film bearing test rig components, the rotor and housing masses of the ALC test rig were designed to have a similar ratio to that of the FFBTR (refer to Tables II and III).

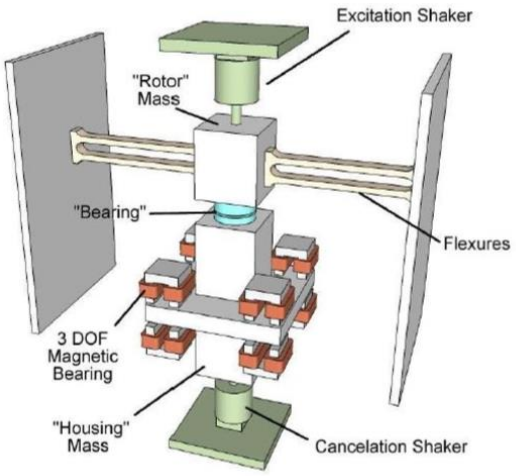


Figure 5: Conceptual Design of Active Load Cell Test Rig

## TEST RIG SIMULATION

A full simulation of the Active Load Cell test rig as depicted in Figure 4 was developed in order to analyze the capabilities of the test rig prior to manufacture. Due to the fact that the exact load at the bearing and bearing properties are known in the simulation model, and all signals are available for evaluation, the use of the simulation model is advantageous in helping to understand the full capabilities of the active load cell concept. The overall system was modeled in Simulink to enable time-transient simulation experiments. This allows for realistic representation of the operation and performance of the overall Active Load Cell system.

Magnetic suspension of the housing is achieved through a classical PID feedback control scheme. Each of the four sets of actuators in either corner of the housing mass are controlled independently, as depicted in Figure 6. The current into the upper and lower actuators on any particular actuator set are dictated by a single sensor and PID control loop. The sensor measures the gap and compares this value to a reference. The controller in turn outputs a control voltage, which produces a current and corresponding force to keep the housing centered.


Figure 6: Housing Suspension Control (side view)

The primary objective of the Active Load Cell is to counter the effects of the dynamic excitation force on the housing such that the acceleration of the housing approaches zero. This cancellation is achieved via an adaptive open-loop control algorithm [6], which superimposes an additional synchronous force on top of the feedback stabilization control loop. This open-loop control force can be altered as the characteristics (frequency, amplitude, phase) of the applied dynamic force are changed without any impact on the magnetic actuator feedback stabilization controller. This is due to the fact that the open-loop control force is effectively an external disturbance force, from the perspective of the stabilization control loop. And therefore, the result is a forced response behavior of the feedback stabilization control system, which does not affect system stability.

In order to ensure optimal performance of the force cancellation control loop, an iterative method is used to adapt the forces to reach a predetermined performance goal (minimize housing acceleration). This cancellation controller is referred to as adaptive open-loop control [9], which has been well documented by R.W. Hope and C.R. Knospe [10] with more experimental results reported in Knospe et al. [6].

The implementation of the adaptive open-loop control algorithm in this application is as follows:

1. Run the simulation under an external harmonic excitation load but with no input to the cancellation shaker and observe the resulting acceleration.
2. Determine the amplitude and phase of the acceleration using a Fourier transform (obtain $x_0$).
3. Define a batch of arbitrary control inputs, $u_i$ (cancellation shaker forces). Run the simulation at each input and observe the resulting acceleration, $x_i$.
4. Calculate the influence coefficient matrix (T): T = X/U.
5. Define the first adaptive input into the cancellation shaker using $u_{i+1} = T_1 x_i$
6. Observe the resulting acceleration, $x_{i+1}$ and repeat the iterative process until the value has effectively converged to zero (i.e. the sensor noise floor).

## SIMULATION RESULTS

Due to variations in the system gain when excited at different frequencies, the system response may result in an unacceptably high or low amount of relative motion. Figure 7 shows how the system response varies as a function of test frequency for a constant pk-pk force amplitude. If the system's response is small compared with the displacement sensor's resolution, the uncertainty of the identification scheme will increase significantly. Therefore, it is useful to adjust the excitation force amplitudes in order to achieve a consistent relative displacement for all excitation frequencies. The result of this process is a Force-Frequency relationship curve, which can be used in the test cases to ensure the applied load is appropriate for each given frequency. For the purposes of this test rig, the target relative motion was chosen to be 0.005 mm. Figure 8 depicts the compensated dynamic forcing function which results in a consistent relative displacement at all test frequencies.

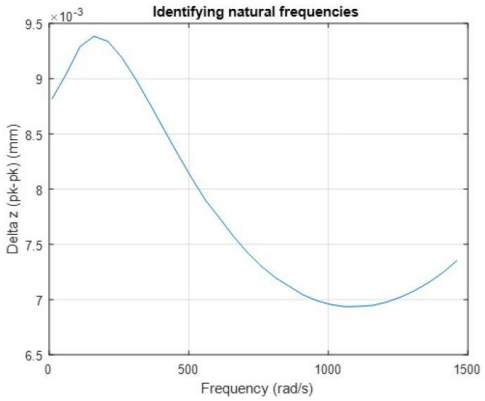


Figure 7. Displacement vs. frequency for a fixed input force

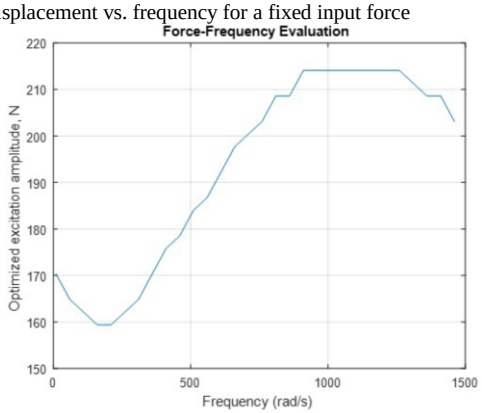


Figure 8. Force vs. frequency for a constant displacement amplitude

In order to validate the simulation model and control technique, the simulation model was initially run without the inclusion of any noise or measurement errors. Results of this initial testing demonstrated the feasibility of the concept and an ability to accurately identify the bearing forces with negligible error with respect to truth for frequencies up to 2750 rad/s (440Hz). Analyzing this idealized scenario is useful for an initial proof of concept, but in order to more accurately predict the capabilities of the actual test rig, it is necessary to identify and simulate all sources of potential measurement error which will be present in the actual test rig and observe their effects on the bearing force identification results. Errors can originate from a large variety of sources, such as calibration of equipment, manufacturing tolerances, electronic hardware delays, etc.

Sources of Measurement Error: For the purposes of this work, the sources of error to be analyzed were directly related to all sensor readings associated with the control system and force identification procedure. This best represents the types of errors that would be present in the actual system. The sources of error and error ranges that were included in this study are listed in Table I. For this study, errors within their respective ranges were randomized and applied to the model and a Monte Carlo analysis procedure consisting of 250 test cases was performed. Using the results of these parametric runs, it is possible to observe the statistical distributions of the final force amplitude and phase errors to develop confidence intervals.

Table I. Monte Carlo simulation parameter values

| Error Source | Nom. Val. | Error Range |
|---|---|---|
| **Magnetic Sensor Errors (x4)** | | |
| Sensor Gain [1] | 1.0 | [0.997 1.003] |
| Sensor Offset [2] | 0.0 mm | [-0.1 +0.1] mm |
| Sensor Tilt [2] ($\alpha$ & $\beta$) | 0 deg | [-3.0 +3.0] deg |
| **Actuator Location Errors (x4)** | | |
| Actuator Offset [2] | 0.0 mm | [-0.1 +0.1] mm |
| **Accelerometer Errors** | | |
| Sensor Gain [1] | 1.0 | [0.95 1.05] |
| Sensor Phase | 0.0 deg | [0.0 2.0] deg |
| Sensor Noise [1] | 0.0 $m/s^2$ (RMS) | [0.005] $m/s^2$ (RMS) |
| Sensor Cross-talk [1] ($X$ & $Y$) | 0.0 % | [-5.0 +5.0] % |
| Sensor Tilt [2] ($\alpha$ & $\beta$) | 0 deg | [-3.0 +3.0] deg |

The stiffness range of bearings to be identified by the final FFBTR is roughly $7.0 \times 10^7 - 3.5 \times 10^8$ N/m (400,000 - 2,000,000 lbf/in). In order to begin to understand the bearing force identification capability of the ALC test rig, two bearing test cases with stiffnesses towards either end of this range were chosen to be analyzed. However, due to different equipment masses (between the ALCTR and FFBTR), it was necessary to find a method to determine a suitable equivalent stiffness range for the ALC test rig. As a first approximation, the natural frequency of the two-mass system joined by a spring was used as the approximation method. The natural frequency of this system can be determined by:

$$k(m_1 + m_2) = (m_1 m_2)\, \omega_n^2 \qquad (15)$$

For the lower and upper stiffness values, the natural system frequency was calculated and used to determine an equivalent stiffness for the ALC test rig, which resulted in the same natural frequency. As displayed in Table III, the equivalent ALC stiffness range is approximately $2.7 \times 10^7$ - $1.3 \times 10^8$ N/m

(154,000 - 742,000 lbf/in). Two test bearings were chosen to study, one at each end of this bearing stiffness range.

The "soft" bearing (Bearing 1) was modeled with the following parameters:

- Stiffness: 30,000,000 N/m (171,000 lbf/in)
- Damping: 1500 Ns/m (8.5 lbf s/in)

And the "stiff" bearing (Bearing 2) was modeled using:

- Stiffness: 100,000,000 N/m (571,000 lbf/in)
- Damping: 5000 Ns/m (28.5 lbfs/in)

Table II. Masses of FFBTR and Active Load Cell Test Rig

| Mass | FFBTR | ALCTR |
|---|---|---|
| $m_1$ | 60 kg | 22.319 kg |
| $m_2$ | 50 kg | 20.870 kg |

Table III. Equivalent Active Load Cell Test Rig stiffnesses

| Stiffness (FFBTR) | | $\omega_n$ | Eq. Stiffness (ALCTR) |
|---|---|---|---|
| Low | 7.0E7 N/m | 1602 rad/s | **2.7E7 N/m** |
| High | 3.5E8 N/m | 3582 rad/s | **1.3E8 N/m** |

Test Frequencies: For consistency, all trials were run at each of the frequencies listed in Table IV. These frequencies are within the range of test frequencies expected to be used in conjunction with the fluid film bearing test rig, and were chosen based on a logarithmic scale.

Table IV. Active Load Cell test frequencies

| (rad/s) | (Hz) | (rad/s) | (Hz) |
|---|---|---|---|
| 120 | 19.09 | 1280 | 203.71 |
| 205 | 32.62 | 1800 | 286.47 |
| 300 | 47.74 | 2340 | 372.42 |
| 440 | 70.02 | 2750 | 437.67 |
| 650 | 103.45 | | |

The test cases were run in the following sequence:

1. For the given test frequency and dynamic force amplitude, the model was run with no measurement errors. This was used as a visual check to make sure the displacement caused by the dynamic force was appropriate. Figure 9 shows the uncontrolled housing motion at a test frequency of 650 rad/s (103 Hz).
2. Apply the adaptive open loop controller with no measurement errors present to be sure the identification process is working correctly. Observe the controlled housing response (example is shown in Figure 10 for the same test conditions – 650 rad/s).
3. Once the model has been verified, run the Monte Carlo studies by varying the measurement error values randomly for 250 simulation test cases and recording the cancellation force amplitude and phase errors with respect to the known true bearing force/phase.
4. Build a statistical distribution of the Monte Carlo studies to develop anticipated errors and confidence intervals.

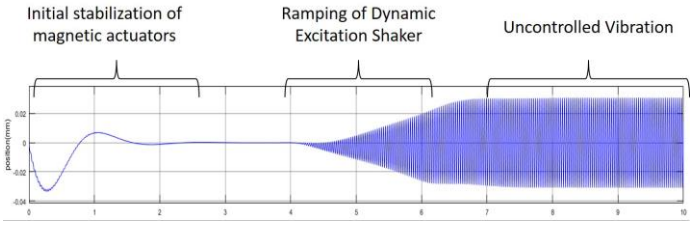


Figure 9. Free housing motion from external force excitation (650 rad/s)

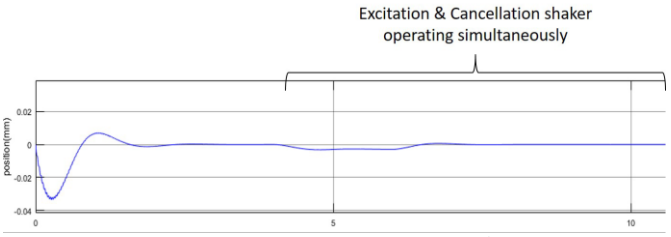


Figure 10: Controlled housing motion under external force excitation (650 rad/s)

An example of the bearing force amplitude and phase error Monte Carlo results for Bearing 1 ("soft" bearing) at a single test frequency (120 rad/s) are shown in Figures 11 and 12. Figures 13 through 16 graphically depict the results for the two test bearings over the entire test frequency range. Figures 13 through 14 show the median errors and limits for the 95% confidence bounds for all test frequencies for Bearing 1. Most test cases fall at or below the 1% target force amplitude error, and all test cases are within the 1 degree target phase error. Figures 15 through 16 show the median errors and limits of the 95% confidence bounds for all test frequencies for Bearing 2 ("stiff" bearing). Similar to bearing 1, most force amplitude errors are at or below the 1% target, and all phase errors are below the 1 degree error target.

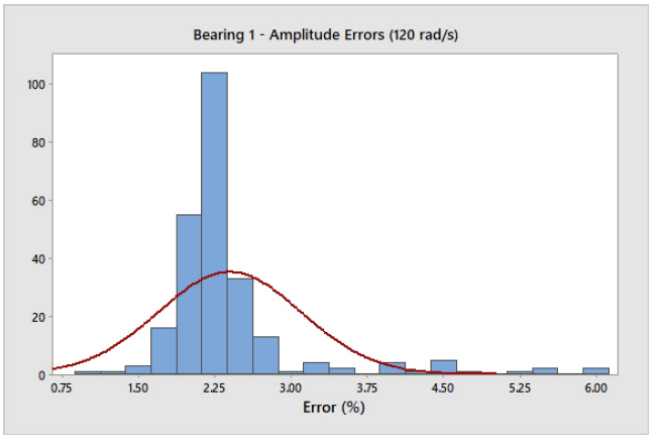


Figure 11: "Soft" bearing Monte Carlo amplitude error distribution (120 rad/s)

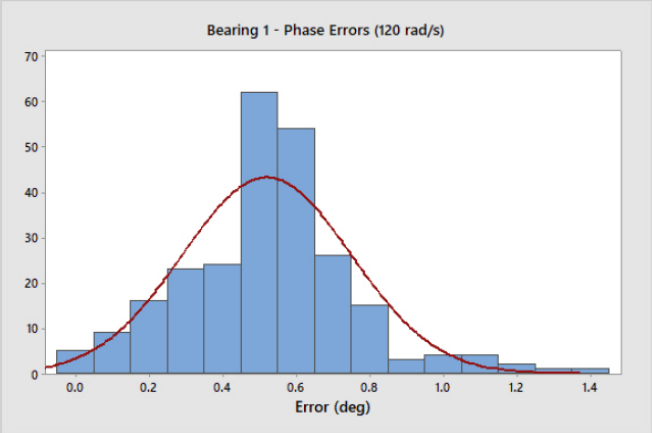


Figure 12: "Soft" bearing Monte Carlo phase error distribution (120 rad/s)

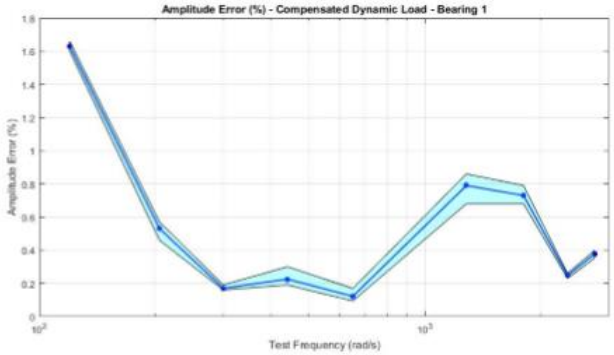


Figure 13: Force amplitude error (%) vs. frequency (Bearing 1)

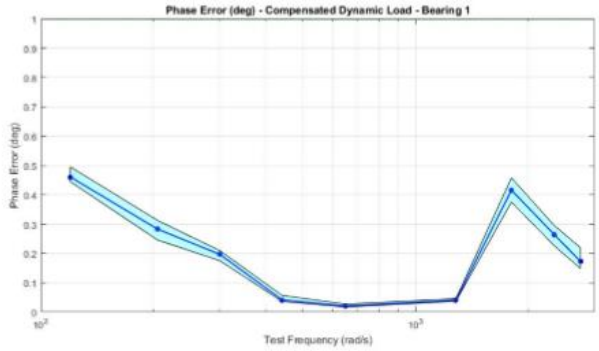


Figure 14: Phase error (deg) vs. frequency (Bearing 1)

## DISCUSSION

### A. *Bearing Force Identification*

A principle goal of this work was to accurately identify the bearing force within 1% of true amplitude, and 1 degree of true phase. Collecting the results for all frequencies, the medians of 81.4% of amplitude measurements and 100% of phase measurements fell within this target. Concatenating all results and error boundaries for each bearing, the following confidence intervals can be established for each experiment (refer to Table V).

From the graphical simulation results depicted in the previous section, it is obvious that the expected errors are

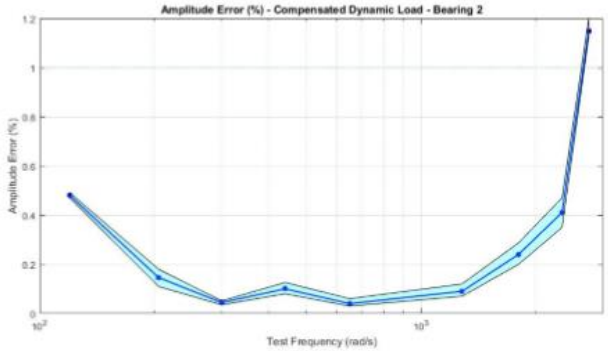


Figure 15: Force amplitude error (%) vs. frequency (Bearing 2)

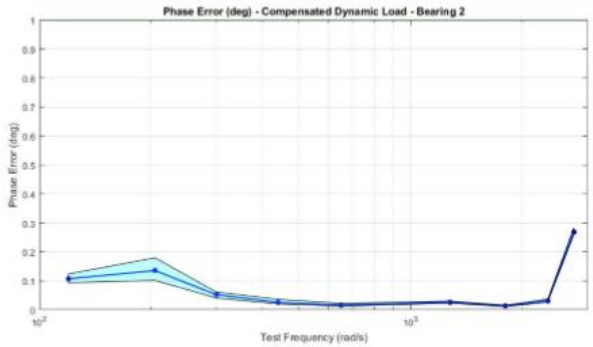


Figure 16: Phase error (deg) vs. frequency (Bearing 2)

Table V. Total amplitude and phase error statistical results

| | Amplitude Error (%) | | | Phase Error (deg) | | |
|---|---|---|---|---|---|---|
| Bearing | Lower | Median | Upper | Lower | Median | Upper |
| 1 (Soft) | 0.3410 | 0.3510 | 0.3700 | 0.1203 | 0.1271 | 0.1340 |
| 2 (Stiff) | 0.3101 | 0.3200 | 0.3410 | 0.0613 | 0.0635 | 0.0676 |

frequency dependent. For example, the median amplitude errors were higher for all cases at 120 rad/s compared with the errors at 205 rad/s, and as such, it can be expected that an experiment run at the lower frequency would result in larger force identification errors. The error ranges were not consistent between bearings, however, larger errors were generally experienced at the lowest and highest test frequencies for each bearing.

### B. *Dynamic Coefficient Identification*

While the ALC test rig has been shown to accurately identify the force at the bearing, the ultimate purpose is to use this force measurement to identify the bearing dynamic coefficients (stiffness and damping). As discussed previously, these coefficients can be determined through the use of the identified bearing force ($F_b$) and the sensed relative displacement ($x_m$) between the rotor and housing (refer to equation (12)).

Similar to the bearing force identification procedure, a Monte Carlo study was performed for the stiffness and damping coefficient identification process. And since the actual stiffness and damping values of the test bearing are known exactly in the simulation model (unlike an actual

bearing test rig), errors in coefficient determination can be directly calculated. This Monte Carlo study was performed at three test frequencies (205, 650 and 2340 rad/s) for both test bearings, and the dynamic coefficient identification error results (median and 95% confidence intervals) are summarized in Table VI.

For both bearings, the identified stiffness values were found to be within 1% of the actual truth values for all test frequencies. This result is significant, and demonstrates the promise of utilizing the Active Load Cell concept for the accurate determination of fluid-film bearing dynamic coefficients.

Although the damping coefficient identification errors are higher than those associated with the stiffness coefficients, the results are also promising (especially at the higher frequency range where the errors are <10%). The largest damping errors occur at the lowest test frequency, which can be attributed to the inherently larger percent errors in the velocity measurements based on displacement sensor readings at lower frequencies.

Table VI. Stiffness and damping identification error results for Bearing 1 & 2

| | | Stiffness (%) | | | Damping (%) | | |
|---|---|---|---|---|---|---|---|
| | | Lower | **Median** | Upper | Lower | **Median** | Upper |
| Bearing 1 | 205 rad/s (all) | 0.440 | **0.500** | 0.563 | 56.200 | **68.100** | 77.410 |
| | 650 rad/s (all) | 0.156 | **0.170** | 0.177 | 2.029 | **2.440** | 3.040 |
| | 2340 rad/s (all) | 0.470 | **0.488** | 0.530 | 2.227 | **2.420** | 2.566 |
| Bearing 2 | 205 rad/s (all) | 0.255 | **0.279** | 0.305 | 58.320 | **66.400** | 74.432 |
| | 650 rad/s (all) | 0.161 | **0.177** | 0.190 | 6.575 | **9.951** | 25.016 |
| | 2340 rad/s (all) | 0.155 | **0.165** | 0.180 | 0.522 | **0.577** | 0.637 |

## CONCLUSIONS

- The analysis presented in this paper suggest that test rigs developed for the identification of dynamic bearing coefficients should strive to measure the force generated by the fluid film more directly.
- If the bearing force can be measured without the need for inertial compensation, the uncertainty in the dynamic coefficients is a linear function of test frequency. This is a significant improvement (especially at higher frequencies) from the quadratic error relationship with respect to test frequency associated with traditional test rig methods.
- An Active Load Cell is proposed as a method to achieve accurate bearing force identification. The results of the simulation study indicate that the Active Load Cell is a very accurate method for determining force amplitude and phase predictions across the tested frequency range (100-3000 rad/s (20-500 Hz)). The overall median error in force amplitude identification was approximately 0.35% for the two bearing examples. And the overall median error in phase identification was approximately 0.12 degrees.
- The results of the stiffness and damping coefficient error study indicate that the Active Load Cell concept may significantly improve the accuracy of bearing dynamic coefficient identification. The trial runs demonstrated coefficient identification which was much more accurate for all stiffness and most damping results than all previous methods of identifying these coefficients [3, 4].
- The simulation study results strongly suggest that in addition to its use within a FFBTR, the Active Load Cell could be very beneficial as a standalone test rig capable of the accurate identification of unknown dynamic forces more generally.


## ACKNOWLEDGEMENTS

This work was funded by the Rotating Machinery and Control (ROMAC) Laboratories at the University of Virginia.


## REFERENCES


[1] M. He, "Thermoelastohydrodynamic analysis of fluid film journal bearings," PhD dissertation, 2004.

[2] J.A. Kocur, J.C. Nicholas, and C.C. Lee, "Surveying Tilting Pad Journal Bearing and Gas-Labyrinth Seal Coefficients and Their Effect on Rotor Stability," *Proceedings of the 36th turbomachinery symposium*, 2007.

[3] T.W. Dimond, P.N. Sheth, P. E. Allaire, and M. He, "Identification methods and test results for tilting pad and fixed geometry journal bearing dynamic coefficients – A review," *Shock and vibration*, 16.1, pp. 13-43, 2009.

[4] B. Schwartz, R. Fittro, and C. Knospe, "Understanding the Efect of Systematic Errors on the Accuracy of Experimental Measurements of Fluid-Film Bearing Dynamic Coefficients," *ASME Turbo Expo 2017: Turbomachinery Technical Conference and Exposition*. 2017

[5] G. J. Kostrzewsky, and R. D. Flack, "Accuracy evaluation of experimentally derived dynamic coefficients of fluid film bearings part 1: develompent of method," *Tribology Transactions*, 33.1, pp. 105-114, 1990.

[6] C.R. Knospe, R. W. Hope, S. J. Fedigan, and R. D. Williams, "Experiments in the control of unbalance response using magnetic bearings," *Mechatronics*, 5(4), pp. 385-400, 1995.

[7] C. R. Knospe, and S. M. Tamer, "Experiments in robust control of rotor unbalance response using magnetic bearings," *Mechatronics*, 7.3, pp. 217-229, 1997.

[8] F. Betschon, and C. R. Knospe, "Reducing magnetic bearing currents via gain scheduled adaptive control," *IEEE/ASME transactions on mechatronics*, 6.4, pp. 437-443, 2001.

[9] C. Knospe, "Reducing unbalance response with magnetic bearings," *Int, Rep., Center for Magnetic Bearings*, 1992.

[10] C.R. Knospe, R.W. Hope, S.J. Fedigan, R.D. Williams, "New Results in the Control of Rotor Synchronous Vibration", *Proceedings of the Fourth International Symposium on Matnetic Bearings*, 1994.

[11] P. Gancitano, "Development and Simulation of an Active Load Cell Test Rig", MS Thesis, University of Virginia, 2017.